

β -delayed proton emission from ^{11}Be in effective field theory

Wael Elkamhawy,^{1,*} Zichao Yang,^{2,†} Hans-Werner Hammer,^{1,3,‡} and Lucas Platter^{2,4,§}

¹*Institut für Kernphysik, Technische Universität Darmstadt, 64289 Darmstadt, Germany*

²*Department of Physics and Astronomy, University of Tennessee, Knoxville, TN 37996, USA*

³*ExtreMe Matter Institute EMMI, GSI Helmholtzzentrum für Schwerionenforschung GmbH, 64291 Darmstadt, Germany*

⁴*Physics Division, Oak Ridge National Laboratory, Oak Ridge, TN 37831, USA*

(Dated: October 29, 2020)

We calculate the rate of the rare decay ^{11}Be into $^{10}\text{Be} + p + e^- + \bar{\nu}_e$ using Halo effective field theory, thereby describing the process of beta-delayed proton emission. We assume a shallow $1/2^+$ resonance in the $^{10}\text{Be}-p$ system with an energy consistent with a recent experiment by Ayyad *et al.* and obtain $b_p = 4.9_{-2.9}^{+5.6}(\text{exp.})_{-0.8}^{+4.0}(\text{theo.}) \times 10^{-6}$ for the branching ratio of this decay, predicting a resonance width of $\Gamma_R = (9.0_{-3.3}^{+4.8}(\text{exp.})_{-2.2}^{+5.3}(\text{theo.}))$ keV. Our calculation shows that the experimental branching ratio and resonance parameters of Ayyad *et al.* are consistent with each other. Moreover, we analyze the general impact of a resonance on the branching ratio and demonstrate that a wide range of combinations of resonance energies and widths can reproduce branching ratios of the correct order. Thus, no exotic mechanism (such as beyond the standard model physics) is needed to explain the experimental decay rate.

Introduction. Halo nuclei display a large separation of scales between a few loosely bound halo nucleons and a tightly bound core [1–4]. The emergence of the halo degrees of freedom is a fascinating aspect of nuclei away from the valley of stability. It can be considered a consequence of the quantum tunneling of halo neutrons out of the core potential to the classically forbidden region. This separation of scales can be used to treat these systems using an effective field theory (EFT) approach called Halo EFT [5–7]. Common to all EFTs is that observables are described in a systematic low-energy expansion and that the accuracy of a calculation can be systematically improved. Halo EFT has been applied to a number of observables, including electromagnetic capture reactions and photodissociation processes [8–14].

Here we will consider, for the first time, the weak decay of the valence neutron of the halo nucleus ^{11}Be into the continuum, $^{11}\text{Be} \rightarrow ^{10}\text{Be} + p + e^- + \bar{\nu}_e$, within Halo EFT.

First experimental results for this rare decay mode were presented in Refs. [15, 16]. Riisager *et al.* [17] measured a surprisingly large branching ratio for this decay process, $b_p = 8.3(9) \times 10^{-6}$, which could only be understood in their Woods-Saxon model analysis if the decay proceeds through a new single-particle resonance in ^{11}B . Their measured branching ratio is also more than two orders of magnitude larger than the cluster model prediction by Baye and Tursunov [18]. This led Pfützner and Riisager [19] to suggest that β -delayed proton emission in ^{11}Be is also a possible pathway to detect a dark matter decay mode as proposed by Fornal and Grinstein [20]. More recently, this branching ratio was remeasured by Ayyad *et al.* [21] as $b_p = 1.3(3) \times 10^{-5}$, similar in size to the previous measurement. They also presented new evidence for a low-lying resonance in ^{11}B with resonance energy $E_R = 0.196(20)$ MeV and width $\Gamma_R = 12(5)$ keV. Using these parameters, the authors calculated the decay rate in a Woods-Saxon model assuming a pure Gamow-

Teller transition. They obtained $b_p = 8 \times 10^{-6}$, which has the correct order of magnitude but is only consistent within a factor of two with their experimental result. The work by Ayyad *et al.* was criticized in a recent comment by Fynbo *et al.* [22]. A new experiment by Riisager *et al.* [23] gives an upper limit of $b_p \leq 2.2 \times 10^{-6}$ for the branching ratio but some questions remain due to inconsistencies between different measurements. In conclusion, the branching ratio for β -delayed proton emission in ^{11}Be remains an important unsolved problem.

The ground state of ^{11}Be is a well-understood S -wave halo nucleus. From the ratio of the one-neutron separation energy of ^{11}Be and the excitation energy of the ^{10}Be core, one can extract the expansion parameter for a description with the core and valence neutron as effective degrees of freedom, $R_{\text{core}}/R_{\text{halo}} \approx 0.4$ [8]. Here R_{core} and R_{halo} are the length scales of the core and halo, respectively. In principle, both the ^{10}Be core and the halo neutron can β -decay. Since the half-life of the neutron ($T_{1/2} = 10$ min) is much shorter than the half-life of the core ($T_{1/2} = 10^6$ a), it is safe to assume that for β -delayed proton emission it is always the halo neutron that decays in the halo picture. Therefore, one would naively expect the nucleus to emit this proton due to the repulsive Coulomb interaction: $^{11}\text{Be} \rightarrow ^{10}\text{Be} + p + e^- + \bar{\nu}_e$. This process, called β -delayed proton emission, has well-defined experimental signatures. However, it is also known that short-distance mechanisms such as the decay into excited states of ^{11}B (that are beyond the halo interpretation) dominate the total β -decay rate of ^{11}Be [24, 25].

Halo EFT offers a new perspective on β -delayed proton emission from ^{11}Be by providing a value for the decay rate with a robust uncertainty estimate. It uses the appropriate degrees of freedom and parametrizes the decay observables in terms of a few measurable parameters. Thus, it is perfectly suited for the theoretical description

of low-energy processes such as β -delayed proton emission from halo nuclei. Kong and Ravndal [26] used these ideas to successfully describe the inverse process of pp -fusion into a deuteron and leptons. In contrast to the previous calculation in Ref. [18], we will use new experimental input parameters and put additional emphasis on the uncertainties associated with using effective degrees of freedom. The halo neutron can β -decay through both the Gamow-Teller and Fermi operators. The Fermi operator can only connect states in the same isospin multiplet. If all neutrons in ^{11}Be contribute to the β -decay, this implies that the final state must have $T = 3/2$. No such states are currently known in ^{11}B within the β -decay window. However, due to the halo character of ^{11}Be we expect that only the halo neutron decays, such that the final state has no definite isospin. Thus, we will keep our analysis general and consider both the scenarios of Gamow-Teller and Fermi decay as well as a pure Gamow-Teller decay in the following. Specifically, we will show that based on the measured branching ratio, a low-lying resonance is the likely reason for the large partial decay rate, confirming the suggestion of Ref. [17]. Furthermore, in ^{11}B , we explore the impact of the resonance energy and width on the decay rate and show that the recent results for the resonance energy and width of a low-lying resonance are consistent with the experimentally measured branching ratio.

In order to keep our presentation self-contained, we start by summarizing the concepts of Halo EFT for S -wave halo nuclei. We discuss the calculation of decay rates with and without strong final state interactions and then display our results. We conclude with a summary.

Theoretical foundations. The Halo EFT Lagrangian \mathcal{L} for ^{11}Be as well as the low-lying resonance in ^{11}B up to next-to-leading order can be written as $\mathcal{L} = \mathcal{L}_0 + \mathcal{L}_d$, where \mathcal{L}_0 is the free Lagrangian of the ^{10}Be core, neutron and proton

$$\begin{aligned} \mathcal{L}_0 = & c^\dagger \left(i\partial_t + \frac{\nabla^2}{2m_c} \right) c + n^\dagger \left(i\partial_t + \frac{\nabla^2}{2m_n} \right) n \\ & + p^\dagger \left(i\partial_t + \frac{\nabla^2}{2m_p} \right) p, \end{aligned} \quad (1)$$

with c , n and p the core, neutron and proton fields, respectively. The masses of core, neutron and proton are denoted by m_c , m_n and m_p . The S -wave core-neutron as well as core-proton interaction are described by \mathcal{L}_d , which reads

$$\begin{aligned} \mathcal{L}_d = & d_{\text{Be}}^\dagger \left[\eta \left(i\partial_t + \frac{\nabla^2}{2M_{nc}} \right) + \Delta \right] d_{\text{Be}} \\ & + d_{\text{B}}^\dagger \left[\tilde{\eta} \left(i\partial_t + \frac{\nabla^2}{2M_{pc}} \right) + \tilde{\Delta} \right] d_{\text{B}} \\ & - g [c^\dagger n^\dagger d_{\text{Be}} + \text{H.c.}] - \tilde{g} [c^\dagger p^\dagger d_{\text{B}} + \text{H.c.}], \end{aligned} \quad (2)$$

where d_{Be} and d_{B} are spinor fields, with spin indices suppressed, that represent the $J^P = 1/2^+$ ground state of

^{11}Be and the $J^P = 1/2^+$ low-lying resonance in ^{11}B , respectively, while $M_{nc} = m_n + m_c$ and $M_{pc} = m_p + m_c$.

The renormalization of the low-energy constants for ^{11}Be has been discussed in Ref. [8]. Here, we will briefly summarize the relevant results to define our notation. Due to the non-perturbative nature of the interaction, we need to resum the self-energy diagrams to all orders. After matching the low-energy constants for ^{11}Be appearing in Eq. (2) to the effective range expansion, we obtain the full two-body T-matrix

$$T_0(E) = \frac{2\pi}{m_R} \left[\frac{1}{a_0} - r_0 m_R E - \sqrt{-2m_R E - i\epsilon} \right]^{-1}. \quad (3)$$

where m_R is the reduced mass, and a_0 , r_0 are the S -wave $^{10}\text{Be}-n$ scattering length and effective range, respectively. The residue at the bound state pole of Eq. (3) is required to calculate physical observables, $Z = \frac{2\pi\gamma_0}{m_R^2} / (1 - r_0\gamma_0)$, with $\gamma_0 = (1 - \sqrt{1 - 2r_0/a_0})/r_0 \equiv \sqrt{2m_R S_n}$ the binding momentum of the S -wave halo state, and S_n the one-neutron separation energy of the halo nucleus.

In order to investigate β -delayed proton emission from ^{11}Be , we include the weak interaction current allowing transitions of a neutron into a proton, electron and antineutrino which corresponds to the hadronic one-body current. Moreover, we have to consider hadronic two-body currents that appear in the dimer formalism once the effective range is included. The corresponding Lagrangian is given by

$$\mathcal{L}_{\text{weak}} = -\frac{G_F}{\sqrt{2}} l_-^\mu \left((J_\mu^+)^{1b} + (J_\mu^+)^{2b} \right), \quad (4)$$

where $l_-^\mu = \bar{u}_e \gamma^\mu (1 - \gamma^5) v_{\bar{\nu}}$ and $(J_\mu^+)^{1b} = (V_\mu^1 - A_\mu^1) + i(V_\mu^2 - A_\mu^2)$ denote the leptonic and hadronic one-body currents, respectively. Here the hadronic one-body current is decomposed into vector and axial-vector contributions. At leading order, the contributions to this current are $V_0^a = N^\dagger \frac{\tau_a}{2} N$, $A_k^a = g_A N^\dagger \frac{\tau_a}{2} \sigma_k N$, where $|g_A| \simeq 1.27$ is the ratio of the axial-vector to vector coupling constants [27]. Terms with more derivatives and/or more fields (many-body currents) will appear at higher orders. The first and second term give the conventional Fermi and Gamow-Teller operators, respectively. The two-body current is also decomposed into vector and axial-vector contributions and reads

$$(J_\mu^+)^{2b} = \begin{cases} -d_{\text{B}}^\dagger d_{\text{Be}} & \mu = 0, \\ g_A d_{\text{B}}^\dagger \sigma_k d_{\text{Be}} & \mu = k = 1, 2, 3. \end{cases} \quad (5)$$

Weak matrix element and decay rate. We ignore recoil effects in the β -decay and take both the Gamow-Teller and Fermi transitions into account. After lepton sums, spin averaging, and partial phase space integration,

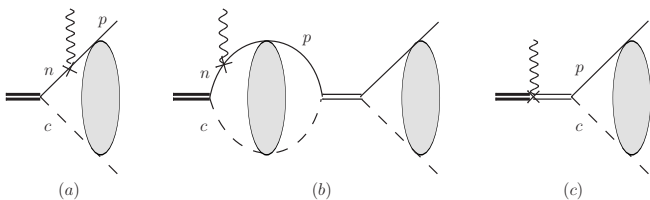


Figure 1. (a): Feynman diagram for the weak decay of a one-neutron halo nucleus into the corresponding core and a proton with Coulomb final state interactions only. (b) + (c): Contributions of strong final state interactions. The thin double line in the middle denotes the dressed $^{10}\text{Be}-p$ propagator. The shaded ellipse denotes the Coulomb Green's function.

we obtain the decay rate

$$\Gamma = \frac{G_F^2(1+3g_A^2)}{4\pi^5} \int dp \int dp_e p^2 p_e^2 (E_0 - E - E_e)^2 \times C^2(\eta_e) |\overline{\mathcal{A}(\mathbf{p})}|^2 \Theta(E_0 - E - E_e), \quad (6)$$

where \mathcal{A} is the *reduced* hadronic amplitude for Gamow-Teller and Fermi transitions whose operator coefficients have been factored out and Θ is the Heaviside step function. Moreover, \mathbf{p} is the relative momentum of the outgoing proton and core, while $E = p^2/(2m_R)$ is their kinetic energy. Furthermore, $E_0 = \Delta m - S_n$, where $\Delta m = 1.29$ MeV is the mass difference between neutron and proton, and $E_e = \sqrt{m_e^2 + p_e^2}$ is the energy of the electron.

The Sommerfeld factor of the electron is given by

$$C^2(\eta_e) = \frac{2\pi\eta_e}{(e^{2\pi\eta_e} - 1)}, \quad (7)$$

where $\eta_e = \alpha Z Z_e E_e / |\mathbf{p}_e|$ with $\alpha = 1/137$ the fine structure constant. We use $Z = Z_p$ in order to ensure that we reproduce the free neutron decay width in the limit of a vanishing one-neutron separation energy of ^{11}Be . This means that the electron is only interacting with the outgoing proton. We assume this to be a good approximation since the ^{10}Be core is far away from the decaying valence neutron due to the small one-neutron separation energy. If a pure Gamow-Teller transition is considered, the factor $1 + 3g_A^2$ is replaced by $3g_A^2$. This results in a reduction of the decay rate by 17 %.

Beta-strength sum rule. The so-called Fermi and Gamow-Teller sum rules (also collectively known as beta-strength sum rule) count the number of weak charges that can decay in the initial state. We will require that this beta-strength sum rule is fulfilled at each order within our EFT power counting. For a transition into the continuum, the sum rule is exactly fulfilled when integrating the differential beta-strengths

$$\frac{dB_F}{dE} = \frac{G_F^2}{4\pi^5} m_R \sqrt{2m_R E} \frac{m_e^5 B}{\ln 2}, \quad (8)$$

$$\frac{dB_{GT}}{dE} = 3 \frac{dB_F}{dE}, \quad (9)$$

over the whole continuum where $B = 6147$ s is the β -decay constant [28]. In the halo picture, we therefore expect beta-strengths B_F and B_{GT} to be at most 1 and 3, respectively, when integrating over the available Q -window. The beta-strengths are related to the comparative half-life of a decay, the so-called ft value given by

$$ft = \frac{B}{B_F + g_A^2 B_{GT}}. \quad (10)$$

At LO where the full non-perturbative solution for a zero-range interaction is used in the incoming as well as outgoing channel, the sum rule is always satisfied. At NLO where range corrections are included, the sum rule puts strong constraints on the ranges in the incoming and outgoing channels such that only certain combinations are allowed.

Hadronic current without final state interactions. The amplitude for the charge changing weak transition of a two-body system is illustrated as diagram (a) of Fig. 1. It was first calculated in pionless EFT by Kong and Ravndal [26]. The corresponding hadronic current can be written as [29]

$$\mathcal{A}_C^{(a)}(\mathbf{p}) = -ig\sqrt{Z}C(\eta_p)e^{i\sigma_0} \frac{2m_R}{\mathbf{p}^2 + \gamma_0^2} e^{2\eta_p \arctan(|\mathbf{p}|/\gamma_0)}, \quad (11)$$

where σ_0 is the Coulomb phase and $C^2(\eta_p)$ is the Sommerfeld factor from Eq. (7). In the $^{10}\text{Be} - p$ system, the Sommerfeld parameter is $\eta_p = \alpha Z_p Z_c m_R / |\mathbf{p}|$, with $Z_p = 1$ and $Z_c = 4$.

Hadronic current with final state interactions. The current (11) includes only the final state interaction from the exchange of Coulomb photons. We now consider strong final state interactions whose signature is a low-lying resonance in the $^{10}\text{Be} - p$ channel up to NLO. These contributions are shown as diagrams (b) and (c) of Fig. 1. Diagram (c) contributes only at NLO to the amplitude. It arises from a two-body current (with known coupling strength) that appears as a result of the energy-dependent interactions used in the initial state (see Eq. (2)) and the final state (see Ref. [30]). The thin double line together with the shaded ellipses that represent Coulomb Green's functions as depicted in diagram (b) essentially combine to the strong scattering amplitude T_{CS} given either in Eq. (12) or (18) [26, 30].

The degrees of freedom in Halo EFT are the emitted outgoing proton and ^{10}Be . Our treatment of the resonance follows Ref. [30]. The corresponding strong scattering amplitude modified by Coulomb corrections is [30]

$$T_{CS} = \frac{-4\pi/m_R}{\left(r_C - \frac{1}{3k_C}\right)(p^2 - k_R^2) + \frac{p^2}{3k_C} - 4k_C H(\eta_p)}, \quad (12)$$

where $H(\eta_p) = \text{Re}[\psi(1 + i\eta_p)] - \ln \eta_p + \frac{i}{2\eta_p} C^2(\eta_p)$, with the digamma function $\psi(z)$. The parameters in Eq. (12)

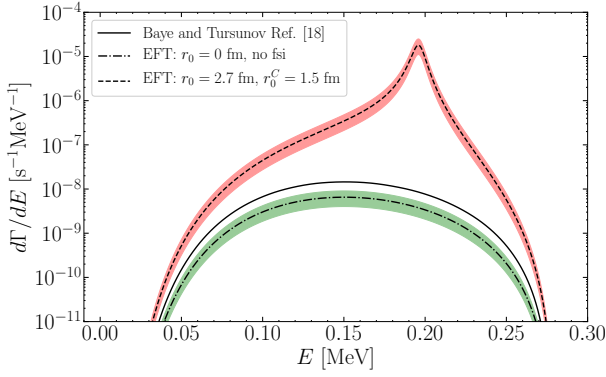


Figure 2. Differential decay rate $d\Gamma/dE$ for β -delayed proton emission from ^{11}Be as a function of the final-state particle energy E . The dash-dotted line shows our EFT result without final state interactions while the solid line gives the result obtained by Baye and Tursunov [18]. The dashed line shows the EFT result including a resonance at $E_R = 0.196$ MeV in the outgoing channel at NLO. The colored bands give the EFT uncertainty.

are directly related to the resonance momentum k_R and width Γ_R :

$$-\frac{1}{a_C} = -\left(r_C - \frac{1}{3k_C}\right) \frac{k_R^2}{2}, \quad (13)$$

$$r_C = -\frac{4\pi k_C}{m_R \Gamma_R} \frac{1}{e^{2\pi k_c/k_R} - 1} + \frac{1}{3k_C}, \quad (14)$$

where a_C and r_C are the Coulomb-modified scattering length and effective range, respectively. The resonance energy is given by $E_R = k_R^2/(2m_R)$.

The diagrams (b) and (c) of Fig. 1 lead to

$$\mathcal{A}_{CS}^{(b)} = -ig\sqrt{Z}4m_R^2 C(\eta_p) e^{i\sigma_0} \mathcal{I} T_{CS}, \quad (15)$$

$$\mathcal{A}_{CS}^{(c)} = -ig\sqrt{Z}4m_R^2 C(\eta_p) e^{i\sigma_0} \left(\frac{\sqrt{r_0 r_0^C}}{8\pi}\right) T_{CS}, \quad (16)$$

with the complex-valued integral

$$\mathcal{I} = \int \frac{d^3\mathbf{q}}{(2\pi)^3} \frac{C^2(\eta_q) e^{2\eta_q \arctan(|\mathbf{q}|/\gamma_0)}}{\mathbf{q}^2 + \gamma_0^2} \frac{1}{\mathbf{p}^2 - \mathbf{q}^2 + i\epsilon}. \quad (17)$$

The total amplitude \mathcal{A} is the sum of the amplitudes with and without resonance $\mathcal{A} = \mathcal{A}_C^{(a)} + \mathcal{A}_{CS}^{(b)} + \mathcal{A}_{CS}^{(c)}$.

At LO, the Coulomb-modified effective range in the $^{10}\text{Be} - p$ system is zero and the amplitude reduces to

$$T_{CS} = -\frac{2\pi}{m_R} \left[\frac{1}{-1/a_C - 2k_C H(\eta_p)} \right]. \quad (18)$$

Results without final state interactions. We consider two scenarios: beta-delayed proton emission with and without final state interactions from a low-lying resonance in ^{11}B . We start with the first scenario and use the one-neutron separation energy of ^{11}Be

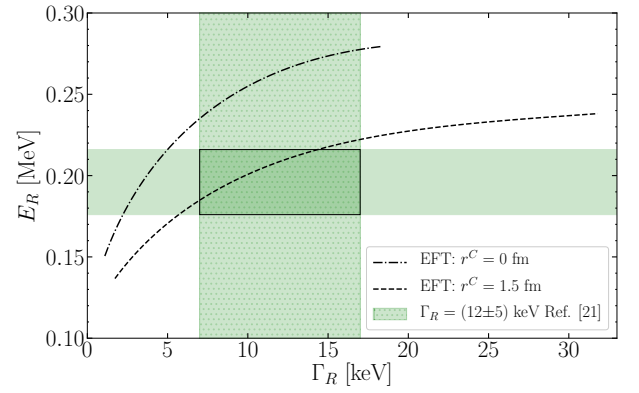


Figure 3. Possible resonance parameter combinations fulfilling the sum rule. The dash-dotted line shows the combinations for $r_0 = 0$ fm at LO corresponding to $r_0^C = 0$ fm while the dashed line shows the combinations for $r_0 = 2.7$ fm at NLO corresponding to $r_0^C = 1.5$ fm. The green bands show the resonance parameters given in Ref. [21].

$S_n = 0.5016$ MeV [25]. In Fig. 2, we plot the differential decay rate $d\Gamma/dE$ as a function of the kinetic energy E of the outgoing hadrons. The solid line gives the result obtained by Baye and Tursunov [18]. The dash-dotted line shows the EFT result with an uncertainty band obtained by adding an uncertainty of order $R_{\text{core}}/R_{\text{halo}} \approx 40\%$ from higher order corrections. The remaining curve includes final state interactions and will be discussed below.

For the branching ratio, we obtain $b_p = \Gamma/\Gamma_{\text{total}} = (1.31 \pm 0.51) \times 10^{-8}$ where the EFT uncertainty is again estimated to be of the order of 40%. Correspondingly, we obtain for the decay rate $\Gamma = (6.6 \pm 2.6) \times 10^{-10} \text{ s}^{-1}$. Baye and Tursunov [18] obtain $\Gamma = 1.5 \times 10^{-9} \text{ s}^{-1}$ which differs by a factor of 2.3 from our result. We note, however, that they used a Woods-Saxon potential with Coulomb interactions tuned to reproduce ^{11}B properties in the final state. Both theoretical results are significantly smaller than the experimental results reported in Refs. [15–17, 21].

Results with final state interactions. We now discuss the second scenario including final state interactions. In Fig. 3, we show the possible resonance parameter combinations that fulfill the beta-strength sum rule. The dash-dotted line is the result at LO where the effective range in the incoming channel as well as the Coulomb-modified effective range in the outgoing channel are zero. At NLO, we use $r_0 = 2.7$ fm determined in Ref. [8] from the measured $B(E1)$ strength for Coulomb dissociation of ^{11}Be . The one-neutron separation energy as well as the effective range of ^{11}Be determine the Coulomb-modified effective range in the outgoing channel to be $r_0^C = 1.5$ fm. The sum rule is then satisfied to very good approximation for a wide range of Coulomb-modified scattering lengths in the outgoing channel. The square shows the experimentally measured resonance pa-

parameter combinations given in Ref. [21]. Our NLO curve depicted as the dashed line exhibits combinations that are in agreement with this measurement as indicated by the overlap of the square and the curve.

In Fig. 4, we show the results for the decay rate as a function of the resonance energy at NLO while using the corresponding resonance width that satisfies the sum rule as shown in Fig. 3. The black line represents the decay rate obtained moving along the NLO curve in Fig. 3 while the red shaded envelope gives the theoretical uncertainty estimated from the counterterm contribution in the axial current scaling with $R_{\text{core}}/R_{\text{halo}} \approx 40\%$. The green bands show the experimentally measured branching ratio and resonance energy of Ref. [21]. The horizontal blue dashed line denotes the result of the model calculation carried out in Ref. [21] whereas the horizontal blue dash-dotted line gives the upper bound of Ref. [23]. Comparing our results with Ref. [23], we find that resonance energies $E_R \geq 0.214$ MeV give results compatible with this upper bound. The corresponding resonance widths can be read off in Fig. 3. When comparing our results with Ref. [21], we find that the low-lying resonance measured in Ref. [21] with $E_R = 0.196(20)$ MeV and width $\Gamma_R = 12(5)$ keV is consistent with their experimentally measured branching ratio as indicated by the overlap of the square and the red shaded band. According to Fig. 3, we determine the width corresponding to the resonance energy $E_R = 0.196(20)$ MeV as $\Gamma_R = (9.0^{+4.8}_{-3.3}(\text{exp.})^{+5.3}_{-2.2}(\text{theo.}))$ keV, which agrees well with the experimental value. Using this value for E_R , we calculate the logarithm of the comparative half-life $\log(ft) = 3.0$ with $B_{\text{GT}} = 2.88$ and $B_{\text{F}} = 0.96$ for a decay including both Gamow-Teller and Fermi transitions and $\log(ft) = 3.1$ with $B_{\text{GT}} = 2.88$ for a pure Gamow-Teller transition. The latter result can be compared to $\log(ft) = 4.8(4)$ calculated by Ayyad *et al.* [21] which was obtained using a pure Gamow-Teller transition as well, but is significantly larger than our result. This large $\log(ft)$ value was also criticized in the comment by Fynbo *et al.* [22]. Ayyad *et al.* corrected the value to $\log(ft) = 2.8(4)$ in their recent erratum [21]. This new value is now in good agreement with our result. Using the half-life for ^{11}Be given in Ref. [25] we convert the Halo EFT result for $E_R = 0.196(20)$ MeV and $\Gamma_R = (9.0^{+4.8}_{-3.3}(\text{exp.})^{+5.3}_{-2.2}(\text{theo.}))$ keV into the final result for the branching ratio $b_p = 4.9^{+5.6}_{-2.9}(\text{exp.})^{+4.0}_{-0.8}(\text{theo.}) \times 10^{-6}$. The corresponding differential decay rate is shown by the dashed line in Fig. 2.

Conclusion. In this paper, we considered β -delayed proton emission from ^{11}Be . We compared the scenario with no strong final state interactions with the scenario of a resonant enhancement in the final $^{10}\text{Be}-p$ channel up to NLO. In the case of no strong final state interactions, we obtained results that are in qualitative agreement with Baye and Tursunov with remaining small dif-

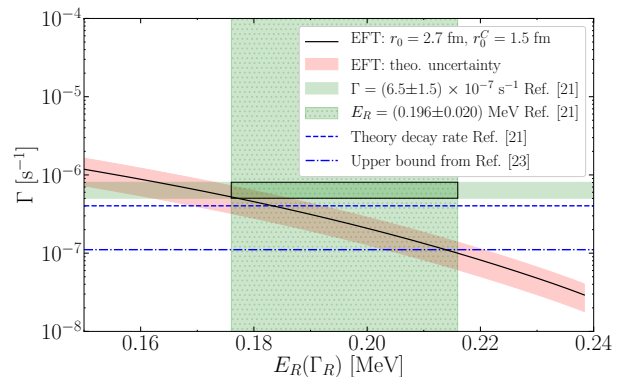


Figure 4. Partial decay rate as a function of the resonance energy at NLO using the corresponding resonance width in accordance with the sum rule (see Fig. 3). Explanation of curves and bands is given in inset.

ferences that can be explained by the different treatment of the final state channel. Including a low-lying resonance with the energy measured in Ref. [21] results in a resonance width and partial decay rate in agreement with this experiment. Thus, our model-independent calculation supports the experimental finding of a low-lying resonance¹. Furthermore, we have explored the sensitivity of the partial decay rate to the resonance energy and decay width and found that this problem is fine tuned, *i.e.* only certain combinations of width and resonance energy can reproduce the partial decay rate. In contrast to the model calculation in Ref. [21], we included both, Fermi and Gamow-Teller transitions. However, if a pure Gamow-Teller decay is considered, their partial decay rate can also be reproduced with slightly smaller resonance parameters. Thus, our result implies that ^{11}Be is not a good laboratory to detect dark neutron decays since no exotic mechanism is needed to explain the partial decay rate.

The uncertainties are largely determined by higher order contributions of the EFT expansion. The next contribution within our power counting that we did not include is a counterterm contribution in the axial current scaling with $R_{\text{core}}/R_{\text{halo}}$. Uncertainties of the S -wave input parameter (the one-neutron separation energy) do not impact the total uncertainty significantly. Therefore, we estimate the uncertainty in the final decay rate to be approximately $R_{\text{core}}/R_{\text{halo}} \approx 40\%$. Experimental data with higher precision could be used to constrain the $^{10}\text{Be}-n$ and $^{10}\text{Be}-p$ interactions. It will be interesting to test whether the inclusion of this resonance changes the Halo EFT predictions for deuteron induced neutron transfer reactions off ^{11}Be which were investigated in Ref. [32].

¹ See Ref. [31] for another recent theoretical calculation in support of this resonance.

We acknowledge useful discussions with T. Papenbrock, M. Madurga and thank D. Baye for providing the data published in Ref. [18]. WE thanks the Nuclear Theory groups of UT Knoxville and Oak Ridge National Laboratory for their kind hospitality and support during his stay. HWH and LP thank the Institute for Nuclear Theory at the University of Washington for its kind hospitality and stimulating research environment. This research was supported in part by the INT's U.S. Department of Energy grant No. DE-FG02-00ER41132. It has been funded by the Deutsche Forschungsgemeinschaft (DFG, German Research Foundation) – Projektnummer 279384907 – SFB 1245, by the German Federal Ministry of Education and Research (BMBF) (Grant no. 05P18RDFN1), by the National Science Foundation under Grant No. PHY-1555030, and by the Office of Nuclear Physics, U.S. Department of Energy under Contract No. DE-AC05-00OR22725.

* elkamhawy@theorie.ikp.physik.tu-darmstadt.de

† zyang32@vols.utk.edu

‡ Hans-Werner.Hammer@physik.tu-darmstadt.de

§ lplatter@utk.edu

- [1] P. G. Hansen, A. S. Jensen, and B. Jonson, *Ann. Rev. Nucl. Part. Sci.* **45**, 591 (1995).
- [2] B. Jonson, *Physics Reports* **389**, 1 (2004).
- [3] K. Riisager, *Phys. Scripta* **T152**, 014001 (2013).
- [4] I. Tanihata, *Eur. Phys. J. Plus* **131**, 90 (2016).
- [5] C. A. Bertulani, H. W. Hammer, and U. Van Kolck, *Nucl. Phys.* **A712**, 37 (2002), [arXiv:nucl-th/0205063](https://arxiv.org/abs/nucl-th/0205063) [nucl-th].
- [6] P. F. Bedaque, H. W. Hammer, and U. van Kolck, *Phys. Lett.* **B569**, 159 (2003), [arXiv:nucl-th/0304007](https://arxiv.org/abs/nucl-th/0304007) [nucl-th].
- [7] H. W. Hammer, C. Ji, and D. R. Phillips, *J. Phys.* **G44**, 103002 (2017), [arXiv:1702.08605](https://arxiv.org/abs/1702.08605) [nucl-th].
- [8] H. W. Hammer and D. R. Phillips, *Nucl. Phys.* **A865**, 17 (2011), [arXiv:1103.1087](https://arxiv.org/abs/1103.1087) [nucl-th].
- [9] G. Rupak and R. Higa, *Phys. Rev. Lett.* **106**, 222501 (2011), [arXiv:1101.0207](https://arxiv.org/abs/1101.0207) [nucl-th].
- [10] E. Ryberg, C. Forssén, H. W. Hammer, and L. Platter, *Eur. Phys. J.* **A50**, 170 (2014), [arXiv:1406.6908](https://arxiv.org/abs/1406.6908) [nucl-th].
- [11] X. Zhang, K. M. Nollett, and D. R. Phillips, *Phys. Lett.* **B751**, 535 (2015), [arXiv:1507.07239](https://arxiv.org/abs/1507.07239) [nucl-th].
- [12] R. Higa, G. Rupak, and A. Vaghani, *Eur. Phys. J.* **A54**, 89 (2018), [arXiv:1612.08959](https://arxiv.org/abs/1612.08959) [nucl-th].
- [13] P. Premarathna and G. Rupak, (2019), [arXiv:1906.04143](https://arxiv.org/abs/1906.04143) [nucl-th].
- [14] X. Zhang, K. M. Nollett, and D. R. Phillips, (2019), [arXiv:1909.07287](https://arxiv.org/abs/1909.07287) [nucl-th].
- [15] M. J. G. Borge, L. M. Fraile, H. O. U. Fynbo, B. Jonson, O. S. Kirsebom, T. Nilsson, G. Nyman, G. Possnert, K. Riisager, and O. Tengblad, *J. Phys.* **G40**, 035109 (2013), [arXiv:1211.2133](https://arxiv.org/abs/1211.2133) [nucl-ex].
- [16] K. Riisager (IS541), *Proceedings, 25th International Nuclear Physics Conference (INPC 2013): Florence, Italy, June 2-7, 2013*, *EPJ Web Conf.* **66**, 02090 (2014).
- [17] K. Riisager *et al.*, *Phys. Lett.* **B732**, 305 (2014), [arXiv:1402.1645](https://arxiv.org/abs/1402.1645) [nucl-ex].
- [18] D. Baye and E. M. Tursunov, *Phys. Lett.* **B696**, 464 (2011), [arXiv:1012.5740](https://arxiv.org/abs/1012.5740) [nucl-th].
- [19] M. Pfützner and K. Riisager, *Phys. Rev.* **C97**, 042501 (2018), [arXiv:1803.01334](https://arxiv.org/abs/1803.01334) [nucl-ex].
- [20] B. Fornal and B. Grinstein, *Phys. Rev. Lett.* **120**, 191801 (2018), [arXiv:1801.01124](https://arxiv.org/abs/1801.01124) [hep-ph].
- [21] Y. Ayyad *et al.*, *Phys. Rev. Lett.* **123**, 082501 (2019), [Erratum: *Phys.Rev.Lett.* 124, 129902 (2020)], [arXiv:1907.00114](https://arxiv.org/abs/1907.00114) [nucl-ex].
- [22] H. O. U. Fynbo, Z. Janas, C. Mazzocchi, M. Pfuetzner, J. Refsgaard, K. Riisager, and N. Sokolowska, (2019), [arXiv:1912.06064](https://arxiv.org/abs/1912.06064) [nucl-ex].
- [23] K. Riisager *et al.*, (2020), [arXiv:2001.02566](https://arxiv.org/abs/2001.02566) [nucl-ex].
- [24] J. Refsgaard, J. Büscher, A. Arokiaraj, H. O. U. Fynbo, R. Raabe, and K. Riisager, *Phys. Rev.* **C99**, 044316 (2019), [arXiv:1811.01620](https://arxiv.org/abs/1811.01620) [nucl-ex].
- [25] J. H. Kelley, E. Kwan, J. E. Purcell, C. G. Sheu, and H. R. Weller, *Nucl. Phys.* **A880**, 88 (2012).
- [26] X. Kong and F. Ravndal, *Nucl. Phys.* **A656**, 421 (1999).
- [27] M. Tanabashi *et al.* (Particle Data Group), *Phys. Rev.* **D 98**, 030001 (2018).
- [28] J. C. Hardy and I. S. Towner, *Phys. Rev.* **C71**, 055501 (2005), [arXiv:nucl-th/0412056](https://arxiv.org/abs/nucl-th/0412056) [nucl-th].
- [29] E. Ryberg, C. Forssén, H. W. Hammer, and L. Platter, *Phys. Rev.* **C89**, 014325 (2014), [arXiv:1308.5975](https://arxiv.org/abs/1308.5975) [nucl-th].
- [30] R. Higa, H. W. Hammer, and U. van Kolck, *Nucl. Phys.* **A809**, 171 (2008), [arXiv:0802.3426](https://arxiv.org/abs/0802.3426) [nucl-th].
- [31] J. Okołowicz, M. Płoszajczak, and W. Nazarewicz, *Phys. Rev. Lett.* **124**, 042502 (2020), [arXiv:1910.12984](https://arxiv.org/abs/1910.12984) [nucl-th].
- [32] M. Schmidt, L. Platter, and H. W. Hammer, *Phys. Rev.* **C99**, 054611 (2019), [arXiv:1812.09152](https://arxiv.org/abs/1812.09152) [nucl-th].